Propagation of finite amplitude sound through turbulence: Modeling with geometrical acoustics and the parabolic approximation

Philippe Blanc-Benon
Laboratoire de Mécanique des Fluides et d'Acoustique, UMR CNRS 5509, BP 163, 69131 Ecully Cedex, France

Bart Lipkens
Mechanical Engineering, Virginia Commonwealth University, Richmond, Virginia 23284-3015

Laurent Dallois
Laboratoire de Mécanique des Fluides et d'Acoustique, UMR CNRS 5509, BP 163, 69131 Ecully Cedex, France

Mark F. Hamilton and David T. Blackstock
Department of Mechanical Engineering, The University of Texas at Austin, Austin, Texas 78712-1063

(Received 26 April 2000; revised 26 June 2001; accepted 26 July 2001)

Sonic boom propagation can be affected by atmospheric turbulence. It has been shown that turbulence affects the perceived loudness of sonic booms, mainly by changing its peak pressure and rise time. The models reported here describe the nonlinear propagation of sound through turbulence. Turbulence is modeled as a set of individual realizations of a random temperature or velocity field. In the first model, linear geometrical acoustics is used to trace rays through each realization of the turbulent field. A nonlinear transport equation is then derived along each eigenray connecting the source and receiver. The transport equation is solved by a Pestorius algorithm. In the second model, the KZK equation is modified to account for the effect of a random temperature field and it is then solved numerically. Results from numerical experiments that simulate the propagation of spark-produced *N* waves through turbulence are presented. It is observed that turbulence decreases, on average, the peak pressure of the *N* waves and increases the rise time. Nonlinear distortion is less when turbulence is present than without it. The effects of random vector fields are stronger than those of random temperature fields. The location of the caustics and the deformation of the wave front are also presented. These observations confirm the results from the model experiment in which spark-produced *N* waves are used to simulate sonic boom propagation through a turbulent atmosphere. [DOI: 10.1121/1.1404378]

PACS numbers: 43.28.Mw, 43.25.Cb [LCS]

I. INTRODUCTION

When finite amplitude (or intense) sound, such as a sonic boom, propagates through a turbulent atmosphere, the propagation can be affected by turbulence. Atmospheric turbulence affects the perceived loudness of sound, mainly by changing its amplitude (peak pressure) and rise time (time portion between 10% and 90% of peak pressure). The results have been of importance for sonic booms because perceived loudness of the sonic boom when heard outdoors[1,2] is a large factor in determining the acceptability of supersonic flight.

Two propagation models are described here that calculate the nonlinear propagation of sound through turbulence. One is based on a geometrical acoustics approach and the other on a parabolic equation, namely, a modified KZK (Khokhlov–Zabolotskaya–Kuznetsov) equation.[3] Both approaches include a turbulence model that is used to generate individual realizations of a homogeneous, isotropic turbulent field.[4] Random temperature and velocity fields are generated. In the geometrical acoustics approach, linear geometrical acoustics is used to trace rays through each realization of the turbulent field. A nonlinear transport equation is then derived for the propagation along the rays. The transport equation is solved by a Pestorius type algorithm.[5] Absorption and dispersion are included in the model. In the second approach, a modified KZK equation that includes the effect of a random temperature field is solved numerically in the time domain. The main motivation for this work is to investigate to what extent finite amplitude effects alter the propagation of sound through turbulence, i.e., to determine the extent to which peak pressure and rise time distribution are altered. Results from numerical simulations of the propagation of spark-generated *N* waves through turbulence are reported.

In the first section, an overview of the turbulence model is presented. Next, the theory of linear geometrical acoustics is reviewed. A calculation of the probability density function of the occurrence of caustics is performed. Then, we derive the nonlinear transport equation along the eigenrays. In Sec. IV, the modification of the KZK equation to include the effect of a random temperature field is presented. Finally, numerical results are presented for the propagation of spark-produced *N* waves through turbulence.

II. TURBULENCE MODEL

Since we assume that the travel time of the acoustic wave through the turbulent medium is much smaller than the evolution time of the turbulent structures, we consider the turbulence frozen. The turbulent field is characterized as a sequence of independent realizations of a random scalar or vectorial field. Since the motivation of this work is a feasibility study, we limited this study to two-dimensional (2D) turbulent fields. We realize that a full 3D modeling of turbulent fields is necessary to accurately capture the effects of turbulence on sound propagation. The velocity $\mathbf{v}$ of a 2D isotropic random velocity field at a given point $\mathbf{x}$ is constructed[4,6] as a sum of N random incompressible Fourier modes, given by

$$\mathbf{v}'(\mathbf{x}) = \sum_{i=1}^{N} \boldsymbol{\mathcal{U}}(\mathbf{K}_i)\cos(\mathbf{K}_i \cdot \mathbf{x} + \phi_i), \qquad \boldsymbol{\mathcal{U}} \cdot \mathbf{K}_i = 0. \tag{1}$$

The direction of the wave vector $\mathbf{K}_i$ and the phase ϕ_i are independent random variables with uniform distributions in order to ensure statistical isotropy and homogeneity. The amplitude of the velocity vector $|\boldsymbol{\mathcal{U}}(\mathbf{K}_i)|$ is determined by the two-dimensional kinetic energy spectrum $E(K)$, where $K = |\mathbf{K}_i|$. For the results presented here we used an energy spectrum based on a Gaussian correlation function and a von Kármán energy spectrum, e.g., as described by Hinze[7] and Pao.[8]

For a field with a Gaussian longitudinal correlation function $f(r) = \exp(-r^2/L^2)$, the length scale L is related to the integral length scale L_f by

$$L_f = \frac{\sqrt{\pi}}{2} L.$$

For 2D Gaussian correlated fields the energy spectrum for velocity is given by

$$E(K) = \tfrac{1}{8} v'^2 K^3 L^4 \exp(-K^2 L^2/4), \tag{2}$$

where v'^2 is the mean square of the velocity fluctuations.

A 2D isotropic random temperature field T' can be constructed in the same way,[4] i.e.,

$$T'(\mathbf{x}) = \sum_{i=1}^{N} \mathcal{T}(\mathbf{K}_i)\cos(\mathbf{K}_i \cdot \mathbf{x} + \phi_i). \tag{3}$$

The energy spectrum for temperature fields is slightly different from the one for the velocity:

$$G(K) = \tfrac{1}{2} \theta'^2 K L^2 \exp(-K^2 L^2/4), \tag{4}$$

where θ'^2 is the mean square of the temperature fluctuations.

For each random field the same discretization of the energy spectrum is used. The length scales for the temperature and the velocity field are equal and the rms values θ' and v' are determined in such a way that the fluctuations of the index of refraction are the same for the scalar and the vectorial random field. At this point we must recall that the fluctuations of the index of refraction μ are related to the fluctuation of temperature T' and to the component v_1' of the velocity fluctuation in the direction of propagation of the incident wave:

$$\mu = -\frac{T'}{2T_0} - \frac{v_1'}{c_0}, \tag{5}$$

where T_0 is the ambient temperature, and c_0 is the ambient speed of sound.

Even though the Gaussian formalism is a very convenient one, it does not result in a realistic spectrum. This spectrum has a very sharp cutoff for high wave numbers, i.e., small turbulence scales, which is not observed in practice. Real spectra usually have a significant inertial range. The energy is not concentrated in structures of sizes roughly equal to L, but, on the contrary, is spread over both larger and smaller turbulent structures with length scales between an inner scale l_0 and an outer scale L_0. Changing the shape of the energy spectrum presents no special difficulty in our turbulence model. The number of Fourier modes is increased to correctly represent the bigger range of wave numbers. For some of the calculations presented here, we used a modified von Kármán spectrum. For 2D temperature fields, the energy spectrum $G(K)$ is written as:

$$G(K) = \frac{2\theta'^2 L_0^{-5/3}}{\Psi\left(1, \frac{1}{6}, \frac{1}{K_m^2 L_0'}\right)} K \left(K^2 + \frac{1}{L_0^2}\right)^{-11/6} \exp\left(-\frac{K^2}{K_m^2}\right), \tag{6}$$

where Ψ is the confluent hypergeometrical function and $K_m = 5.92/l_0$.

III. LINEAR GEOMETRICAL ACOUSTICS

Linear geometrical acoustics is used to trace rays through each realization of the turbulence field. The classical formulation of linear geometrical acoustics[4,9,10] is well known. The step size ds in the integration of the geometrical acoustics equations is a function of the maximum wave number value K_{Max} that we consider in the turbulence energy spectrum and equals $ds = 1/2K_{\mathrm{Max}}$. A fourth-order Runge–Kutta scheme is used to solve the system of differential equations. For source–receiver type problems it is necessary to find the eigenrays that connect source and receiver.

The standard formulations for ray trace equations, such as described by Pierce,[9] are used to trace acoustic rays through each realization of the turbulent field. The ray trace equations can be written in the form of

$$\frac{d\mathbf{x}}{ds} = \frac{1}{N}(\boldsymbol{\nu} + \mathbf{M}), \tag{7}$$

$$\frac{d\mathbf{p}}{ds} = \frac{1}{N}(\boldsymbol{\nabla} N - (\boldsymbol{\nabla} M) \cdot \mathbf{p}), \tag{8}$$

where $\mathbf{x}$ is the position vector of the ray trajectory parametrized by distance s. Here, $\mathbf{p} = p\boldsymbol{\nu}$ is a nondimensional wave vector given by $\mathbf{p} = \mathbf{k}/k_0$ and $k_0 = \omega/c_0$, where $\mathbf{k}$ is the acoustic wave vector. The index of refraction is $N = c_0/c$, where c is the local speed of sound. The Mach number vector is $\mathbf{M} = \mathbf{v}/c$, where $\mathbf{v}$ is the fluid velocity vector.

The ray trajectory is completely determined by the initial conditions and the value of s. For a 2D plane wave the initial conditions are

$$\mathbf{x}(s=0)=\begin{pmatrix}0\\ y_0\end{pmatrix}, \tag{9}$$

$$\mathbf{p}(s=0)=\frac{N}{1+\mathbf{M}\cdot\boldsymbol{\nu}}\begin{pmatrix}1\\ 0\end{pmatrix}. \tag{10}$$

In order to obtain the local ray tube area, which is related to the local intensity of the wave, we need to trace the evolution of the two geodesic elements $\mathbf{R}=(\partial\mathbf{x}/\partial y_0)_s$ and $\mathbf{Q}=(\partial\mathbf{p}/\partial y_0)_s$. The geodesic elements describe the evolution of the wave front along each ray[10] and are given by

$$\frac{d\mathbf{R}}{ds}=\frac{1}{pN}(\mathbf{Q}-\boldsymbol{\nu}\boldsymbol{\nu}\cdot\mathbf{Q})-\frac{1}{N^2}(\boldsymbol{\nu}+\mathbf{M})\mathbf{R}\cdot\boldsymbol{\nabla}N+\frac{1}{N}\mathbf{R}\cdot\boldsymbol{\nabla}\mathbf{M}, \tag{11}$$

$$\frac{d\mathbf{Q}}{ds}=\frac{1}{N}[\mathbf{R}\cdot\boldsymbol{\nabla}\boldsymbol{\nabla}N-\mathbf{R}\cdot(\boldsymbol{\nabla}\boldsymbol{\nabla}\mathbf{M})\cdot\mathbf{p}-(\boldsymbol{\nabla}\mathbf{M})\cdot\mathbf{Q}]$$
$$-\frac{1}{N^2}(\mathbf{R}\cdot\boldsymbol{\nabla}N)[\boldsymbol{\nabla}N-(\boldsymbol{\nabla}\mathbf{M})\cdot\mathbf{p}], \tag{12}$$

with the appropriate initial conditions

$$\mathbf{R}(s=0)=\begin{pmatrix}0\\ 1\end{pmatrix}, \tag{13}$$

$$\mathbf{Q}(s=0)=\frac{\partial p(0)}{\partial y_0}\begin{pmatrix}1\\ 0\end{pmatrix}. \tag{14}$$

In this work we have considered two different random fields:

(1) The case of an inhomogeneous medium exhibiting only temperature fluctuations, called the scalar case; hence Eqs. (7), (8), (11), and (12) can be simplified by making use of $N^2=1+T'/T_0$ and $\mathbf{M}=\mathbf{0}$.
(2) The case of a medium exhibiting only velocity fluctuations, called the vectorial case, and Eqs. (7), (8), (11), and (12) can be simplified by making use of $N=1$.

A shortcoming of the linear solution is the appearance of caustics. When $\mathbf{R}$ vanishes, the pressure becomes infinite. In reality diffraction causes the pressure amplitude to be some finite value. In a turbulent medium, each individual ray reaches a caustic at some distance x from the source. To get information about this distance, we evaluate the probability density function of the occurrence of caustics by making use of the theory developed by Blanc-Benon *et al.*[11] For an initially plane wave propagating through two-dimensional isotropic turbulence, the probability density $P_2(\xi)$ of the distance ξ to the first caustic is

$$P_2(\xi)=\frac{\eta^2}{\sqrt{2\pi}\xi^{5/2}}e^{-\eta^4/6\xi^3}, \tag{15}$$

where η is equal to 1.85, ξ is the normalized distance $\xi=\mathcal{D}_2^{1/3}x$, and $\mathcal{D}_2$ is the diffusion coefficient. The quantity $\mathcal{D}_2$ is related to the effective spectral density $\Phi_{\text{eff}}(K_x,K_y)$ by

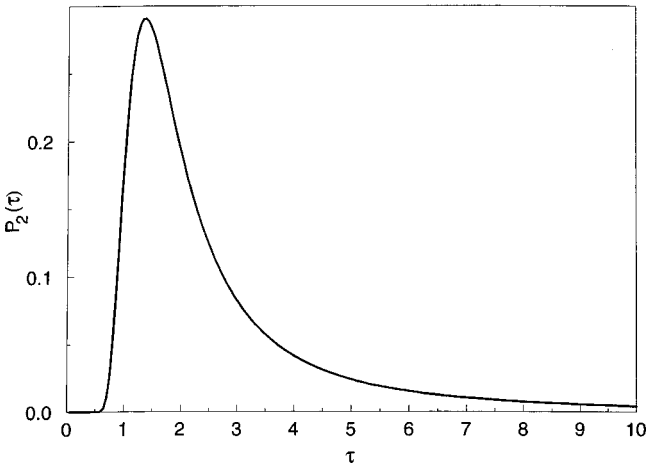

FIG. 1. Probability density function of occurrence of the first caustic for an initial plane wave.

$$\mathcal{D}_2=\pi\int_0^\infty K_y^4\Phi_{\text{eff}}(0,K_y)dK_y, \tag{16}$$

with

$$\Phi_{\text{eff}}(0,K_y)=\Phi_{cc}(0,K_y)+\frac{4}{c_0^2}\Phi_{11}(0,K_y). \tag{17}$$

The spectral density of the temperature fluctuations is Φ_{cc} and the spectral density of the velocity fluctuations v_1' is Φ_{11}. For two-dimensional Gaussian correlations functions of the random medium, it is straightforward to evaluate the diffusion coefficient $\mathcal{D}_2$:

$$\mathcal{D}_2=\mathcal{D}_{2,c}+\mathcal{D}_{2,v}=\frac{12\sqrt{\pi}}{L^3c_0^2}(\sigma_c^2+5\sigma_v^2), \tag{18}$$

where $\sigma_c^2=c_0^2\theta'^2/(4T_0^2)$ and $\sigma_v^2=v'^2$. The contribution to the diffusion coefficient $\mathcal{D}_2$ due to the temperature fluctuation is $\mathcal{D}_{2,c}$ and that due to the velocity fluctuation is $\mathcal{D}_{2,v}$. In Fig. 1 we plot the probability density of occurrence of the first caustic as a function of the normalized distance ξ. For short propagation distances there are no caustics. Then we observe a sharp peak at a fixed distance. The peak of the probability density function occurs at a normalized distance ξ equal to $\sqrt[3]{\eta^4/5}\simeq 1.33$. At larger distances, we observe a decay of the function $P_2(\xi)$ with propagation distance. In the paper by Blanc-Benon *et al.*[4] we showed that this decay is in agreement with the results of Kulkarny and White,[12] and of Klyatskin.[13]

IV. NONLINEAR TRANSPORT EQUATION

A lossless nonlinear transport equation is derived for the propagation of the waves along the eigenrays. Several assumptions are made in the development of the nonlinear equation and are listed here: (1) parameters of inhomogeneity vary slowly on the time scale of the characteristic signal duration, (2) the medium is frozen, i.e., during passage of the acoustic wave the turbulent field is constant in time, (3) self-refraction is not taken into account, i.e., first-order terms are sufficient in the ray equations while second-order terms are only important in describing the transport equation, (4) loss

terms are neglected in the development of the ray path and transport equations, but absorption is added to the numerical algorithm and is dominated by thermoviscous absorption and dispersion of oxygen and nitrogen, (5) the fluid motion is isentropic, (6) ray acoustics approximation is used, (7) weak shock approximation is applied, i.e., only second-order terms are retained in the development of the transport equation.

Starting from the fundamental laws of fluid mechanics and making use of the above stated assumptions, we derive a transport equation. The derivation is lengthy and not presented here, but can be found, e.g., in Robinson.[14] The transport equation for the acoustic pressure p takes the form

$$\frac{\partial}{\partial s}\left[\frac{|A|}{\rho_0 c}|\boldsymbol{\nu}+\mathbf{M}|(1+\mathbf{M}\cdot\boldsymbol{\nu})p^2\right]-\frac{2\beta|A|}{\rho_0^2 c_0^4}p^2 p_{t'}=0, \tag{19}$$

where A is the ray tube area, β is the coefficient of nonlinearity, subscripts 0 denote ambient conditions, and t' is the retarded time coordinate given by $t'=t-\psi(\mathbf{x})$. The effects of passage through a caustic on small-signal waves may be approximated with a $-\pi/2$ phase shift in the frequency domain applied to each frequency component.[15] This is a valid approximation after the wave has passed through the caustic and has propagated back into the small signal domain. It does not present a valid prediction of the wave's behavior in the vicinity of the caustic. The next step is to transform the equation into the form of the homogeneous plane wave case.

First, let $\Pi=Kp'$, where

$$K=\sqrt{\frac{|A|\rho_{0s}c_{0s}}{|A_s|\rho_0 c}|\boldsymbol{\nu}+\mathbf{M}|(1+\mathbf{M}\cdot\boldsymbol{\nu})}, \tag{20}$$

where ρ_{0s}, A_s, and c_{0s} are, respectively, the density, initial ray tube area, and speed of sound at the source. The equation is now written

$$\frac{\partial\Pi}{\partial s}-\frac{\beta|A|\rho_{0s}c_{0s}}{|A_s|\rho_0^2 c_0^4 K^3}\Pi\Pi_{t'}=0. \tag{21}$$

Next, a transformation of the independent variable s, $Z(s)$,[14] is introduced:

$$\frac{dZ}{ds}=\frac{\beta|A|\rho_{0s}c_{0s}}{|A_s|\rho_0^2 c_0^4 K^3}\frac{\rho_{0s}c_{0s}^3}{\beta_{0s}}, \tag{22}$$

and the transport equation now takes the well-known form of Burgers equation[16] for lossless propagation of a finite-amplitude plane wave:

$$\frac{\partial\Pi}{\partial Z}-\frac{\beta_{0s}}{\rho_{0s}c_{0s}^3}\Pi\Pi_{t'}=0. \tag{23}$$

The distortion distance variable $Z(s)$ is given by Eq. (22), which can be rewritten as

$$\frac{dZ}{ds}=\sqrt{\frac{|A_0|}{|A|}\frac{\beta^2}{\beta_0^2}\frac{\rho_0 c_0^5}{\rho c^5}(1+\boldsymbol{\nu}\cdot\mathbf{M})^{-3}|\boldsymbol{\nu}+\mathbf{M}|^{-3}}. \tag{24}$$

The distortion distance variable Z describes the equivalent plane-wave distortion for a wave propagating in a random medium. Equation (23) is integrated numerically along the rays and yields the equivalent distortion value. The Burgers equation is solved numerically by a Pestorius-type algorithm.[5] The nonlinear distortion is applied in the time domain and absorption is applied in the frequency domain.

The computational strategy is then: (1) create realizations of the turbulent field, (2) find eigenrays that connect source and receiver, (3) apply Pestorius algorithm to solve nonlinear transport equation, (4) combine eigenrays to find the waveform at the receiver.

V. MODIFIED KZK EQUATION

Geometrical acoustics is primarily a linear and high frequency approach. Nonlinear effects are taken into account only when solving the nonlinear transport equation along the eigenrays. A second model, described below, was developed to include the effects of diffraction in addition to those of nonlinearity.

Boulanger *et al.*[17] used a turbules approach in which the scattering of sound by each turbule is calculated. The final waveform is calculated by summing over the scattering amplitude of each turbule. Using a Monte Carlo method, Sparrow *et al.*[18] have also studied the influence of atmospheric turbulence on sonic boom propagation, and they discussed the formation of caustics. Other researchers have developed numerical codes derived from discretizations of a wave equation. The latter approach was used in the study of sonic boom propagation in a quiet atmosphere, i.e., in the absence of turbulence.[19,20] The effect of turbulence on finite amplitude sound propagation was studied analytically by Pierce[21] and by Rudenko and Khokhlova.[22]

In order to include diffraction effects, we used the algorithm developed by Lee and Hamilton[3] that solves the KZK equation in the time domain. The KZK parabolic wave equation accounts for diffraction, absorption, and nonlinearity in directional sound fields. We modified the code as described below to include effects of inhomogeneities due to a random temperature field. The KZK equation is expressed here as

$$\frac{\partial p}{\partial z}=\frac{c_0}{2}\int_{-\infty}^{\tau}\nabla_\perp^2 p\,d\tau+\frac{\delta}{2c_0^3}\frac{\partial^2 p}{\partial\tau^2}+\frac{\beta p}{\rho_0 c_0^3}\frac{\partial p}{\partial\tau}, \tag{25}$$

where z indicates the nominal direction of propagation and $\tau=t-z/c_0$ the corresponding retarded time, where c_0 is the mean sound speed in a homogeneous medium. The index 0 denotes the mean values. The total pressure is $P(\mathbf{r},z,t)=P_0+p(\mathbf{r},z,t)$, where P_0 is undisturbed ambient pressure, and the operator $\nabla_\perp^2$ is the projection of the Laplacian in the plane that is normal to the z axis. The constants δ and β are medium-dependent thermoviscous absorption and nonlinearity parameters. Since we consider air at ambient condition, we have $\beta=1.2$. The right part of Eq. (25) is written as a sum over three terms that account for diffraction, relaxation, and nonlinearity. Relaxation due to the absorption in the atmosphere is implemented as done by Cleveland *et al.*[23] In the present investigation we focus on modifying the algorithm to account for inhomogeneity.

To include the effect of turbulence we need to add a term to the KZK equation. In order to reduce computation time, we perform the computations for two-dimensional

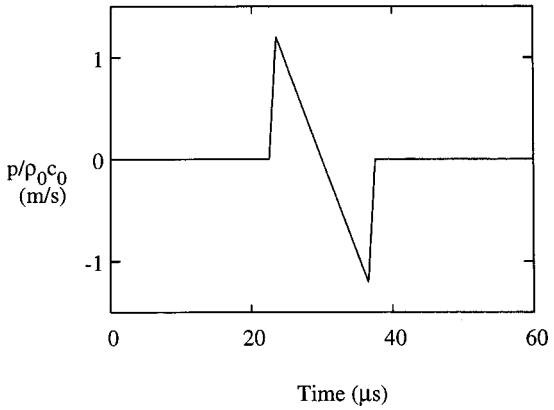

FIG. 2. Input waveform for the numerical experiment with the geometrical acoustics approach.

fields described by the Cartesian coordinates y and z. The effect of the random temperature inhomogeneities is included in the sound speed, and the local sound speed $c(y,z)$ is then written as $c(y,z)=c_0+c'(y,z)$. When the effect of weak sound speed fluctuations is incorporated into the KZK equation, the latter becomes

$$\frac{\partial p}{\partial z}=\frac{c_0}{2}\int_{-\infty}^{\tau}\nabla_{\perp}^2 p\, d\tau+\frac{\delta}{2c_0^3}\frac{\partial^2 p}{\partial \tau^2}+\frac{\beta p}{\rho_0 c_0^3}\frac{\partial p}{\partial \tau}+\frac{c'}{c_0^2}\frac{\partial p}{\partial \tau}. \tag{26}$$

It is this equation that we solved numerically.[3]

Only Gaussian temperature distributions $T(y,z)=T_0+T'(y,z)$ were used to simulate the turbulence. The initial waveform at $z=0$ is a plane N wave, slightly rounded to resemble the waveform produced by an electrical spark. The parameters of the N wave are similar to those used in the geometrical acoustics method.

VI. RESULTS

A. Geometrical acoustics approach

Results are presented for the case of 2D temperature or velocity turbulence fields with a Gaussian longitudinal correlation function, and for the case of a 2D temperature field with a von Kármán spectrum with a significant inertial range (Kolmogorov $-11/3$ law). The Gaussian fields are constructed as a sum of 100 Fourier modes with wave numbers equally spaced between a lower value of $0.1/L$ and a maximum value of $10/L$, where $L=2.5$ cm. In the case of the von Kármán spectrum (Juvé *et al.*[24]) the outer scale L_0 and the inner scale l_0 of turbulence are respectively set to 10 cm and 0.5 cm. The random field is generated with 100 Fourier modes spaced logarithmically between $0.3/L_0$ and $100/L_0$. The refraction index of the two random fields is given by $n=1+\mu$, where μ is the fluctuating part of the refraction index, $\mu=-T'/2T_0-v_1'/c_0$, where T_0 is the ambient temperature. The rms velocity fluctuation in the propagation direction v_1' is 2.5 m/s, and hence the rms temperature fluctuation θ' is 4.27 K. So the rms value of μ is the same for each random velocity or temperature field. Statistics are calculated over 100 realizations.

The initial waveform is that of an N wave similar to that produced by an electrical spark. Peak pressure is 500 Pa, duration is 15 μs, and rise time (time portion between 10% and 90% of peak pressure) is 1 μs (Fig. 2). Spark-produced N waves have been used successfully to simulate the sonic boom propagation through a turbulent atmosphere; see Lipkens.[25–27] The medium is air at ambient conditions with classical thermoviscous absorption, and O_2 and N_2 relaxation are included in the Pestorius algorithm.

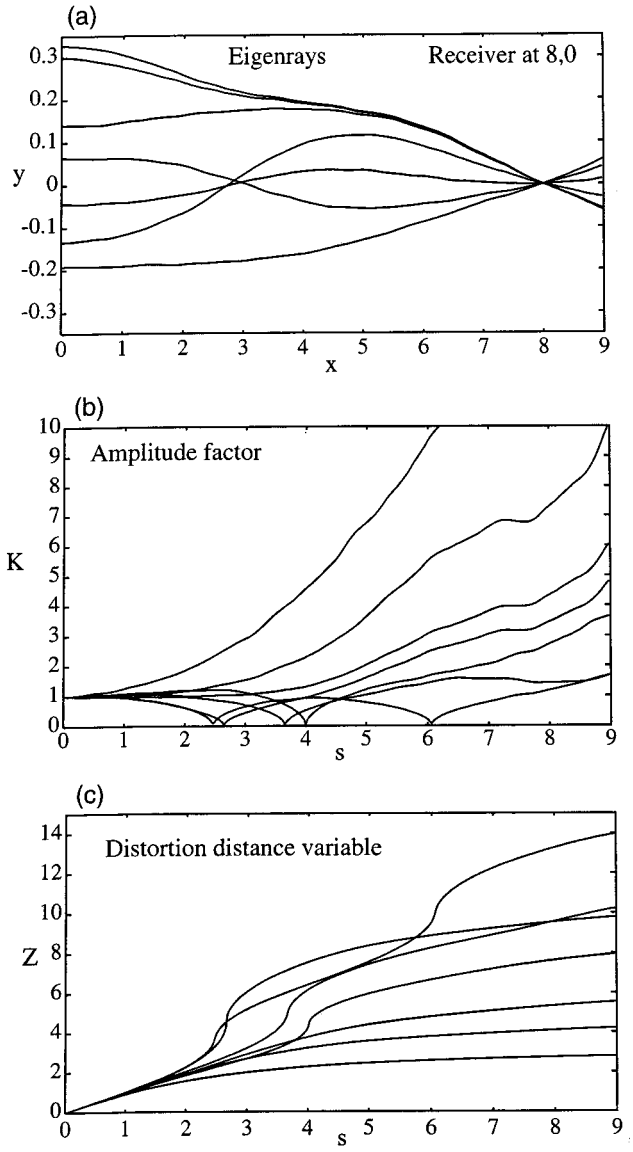

FIG. 3. Calculation example: (a) eigenrays, (b) parameter K, and (c) Z along each eigenray.

In Fig. 3 an example of a typical calculation is shown. In this particular case seven eigenrays [graph (a)] were found that connect the source with the receiver located at a distance of 8 m on the axis. Graph (b) shows the variation of the amplitude factor K along each eigenray. When the eigenray passes through a caustic, the amplitude factor K becomes zero, i.e., an infinite pressure amplitude which is a consequence of the linear geometrical acoustics assumption. The seven eigenrays in Fig. 3(b) can be classified in three categories. We observe that there is one eigenray that passes through two caustics before it reaches the receiver, three rays that pass through one caustic, and three rays did not yet pass

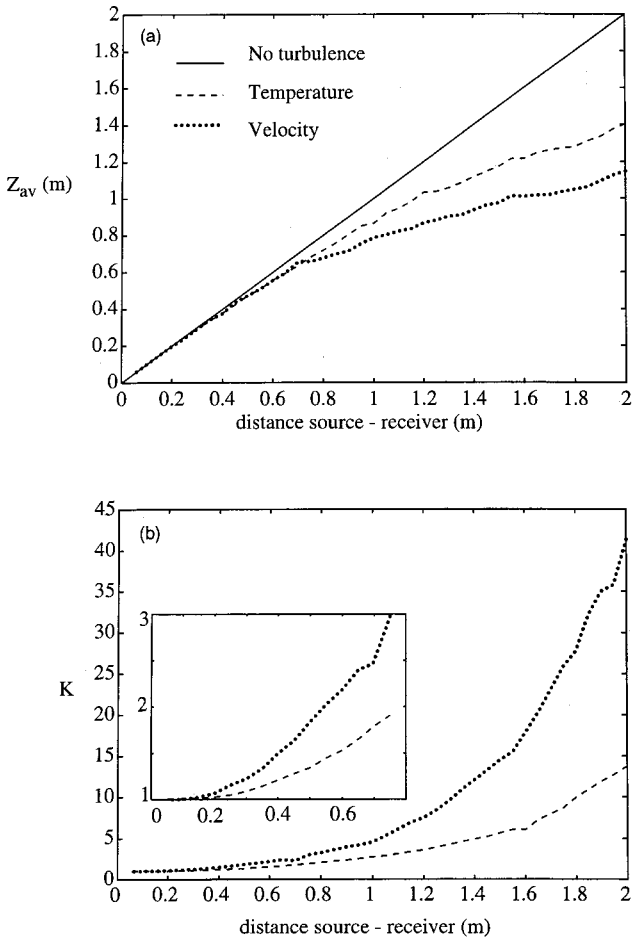

FIG. 4. Averaged results for parameters Z (a) and K (b) for Gaussian turbulent fields. Results are calculated by the geometrical acoustics approach.

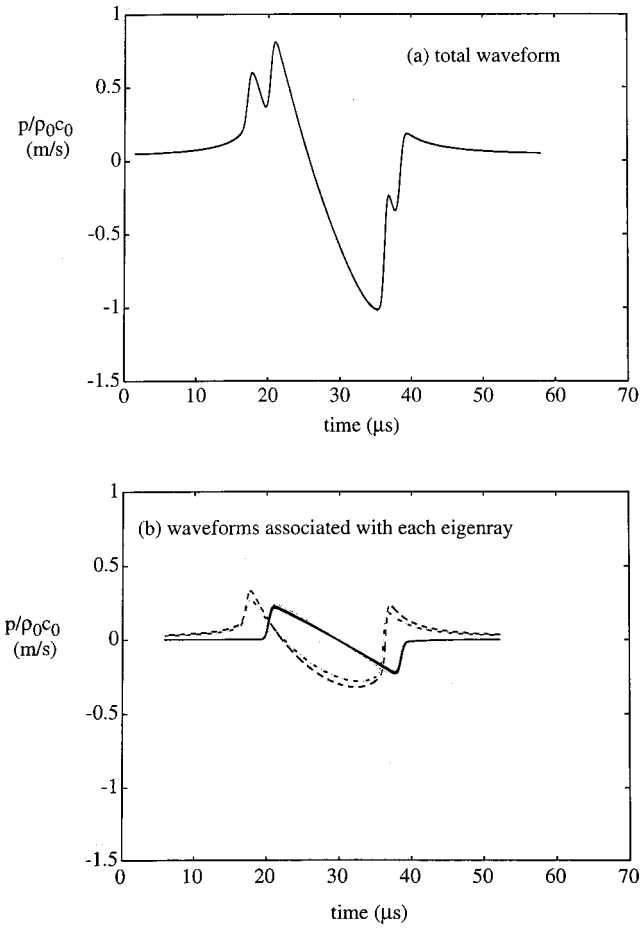

FIG. 5. Example of waveform calculation at the receiver. Graph (a) shows the total waveform and graph (b) shows the waveforms associated with each eigenray.

through a caustic. In graph (c) the distortion distance Z is plotted. For a plane wave in a homogeneous medium we would observe a straight line, i.e., $Z=s$. We see that when the wave passes through the caustic the distortion distance increases more rapidly. After a caustic, the distortion distance grows slower than an equivalent plane wave in a homogeneous medium. For the ray that passed through two caustics, the equivalent distortion distance is nearly 14 m. For one ray that did not propagate through a caustic, the equivalent distortion distance is slightly more than 2 m. The nonlinear

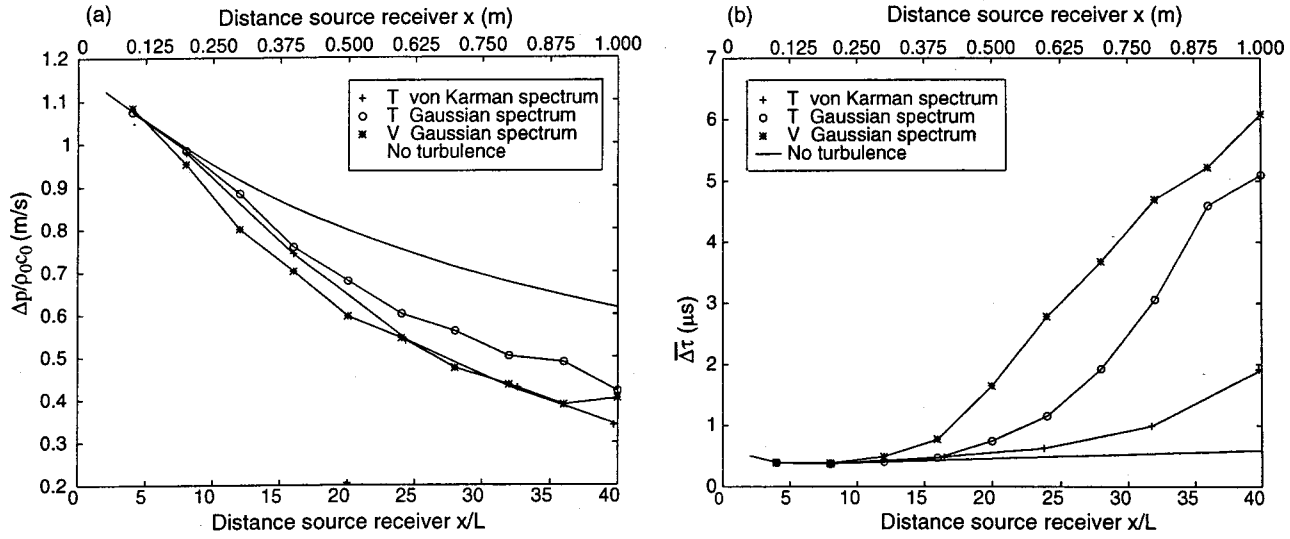

FIG. 6. Averaged normalized values of peak pressure (a) and rise time (b) of the total waveform for 100 realizations are plotted as a function of propagation distance x (m) and normalized propagation distance x/L, where $L=0.025$ m.

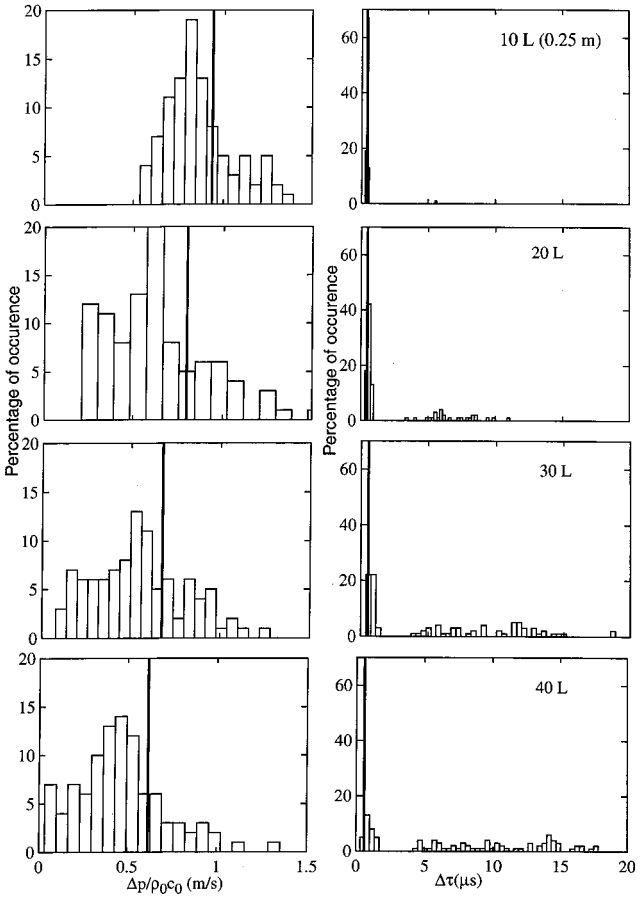

FIG. 7. Histograms of peak pressure and rise time at (a) $10L$, (b) $20L$, (c) $30L$, and (d) $40L$ for the geometrical acoustics model.

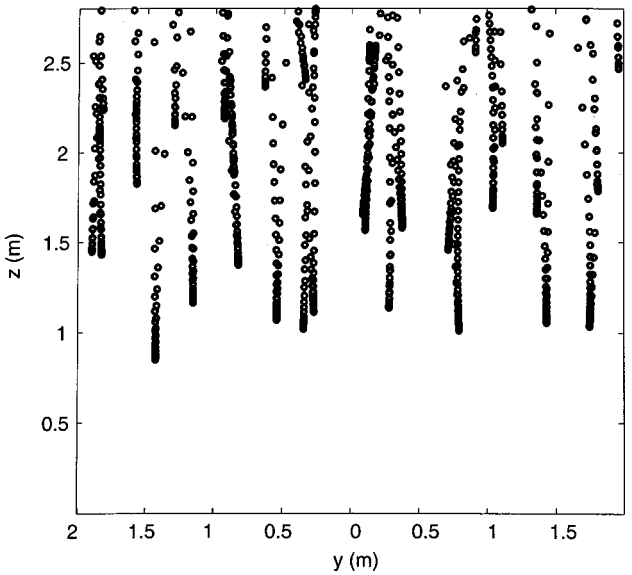

FIG. 8. Location of caustics calculated by the linear geometrical acoustics approach.

distortion will be very weak compared to the homogeneous case. In our previous work, it has been demonstrated that the presence of turbulence always results in a lower value of the age variable Z, i.e., the nonlinear distortion is weaker, and in an increase of the amplitude factor K (Lipkens *et al.*[28,29]).

In Fig. 4 the values of Z and K averaged over 100 realizations of a Gaussian field are presented. In graph (a) the value of Z is shown. Three curves are presented, i.e., for the no turbulence, temperature turbulence, and velocity turbulence cases. It is seen that the presence of turbulence always results in a lower value for the equivalent distortion distance. The effect is more pronounced when propagation distance increases, and stronger for the velocity turbulence. At a propagation distance of $x/L=80$, or $x=2$ m, the equivalent distortion distance for the velocity turbulence is slightly more than 50% than that for no turbulence. Graph (b) presents the values of the amplitude factor K. The factor increases rapidly with propagation distance, an indication that the amplitude of the waveform is less than that of a plane wave having propagated a similar distance in a quiet medium. Again, the effect is more pronounced for the velocity turbulence.

In Fig. 5 an example of a waveform calculation is presented. In this particular case five eigenrays were found that connect source and receiver. The waveform associated with each eigenray is shown in graph (a), while graph (b) shows the global waveform. Two waves have passed through a caustic and the other three have not. The latter three arrive at nearly the same time and are hard to distinguish.

The average values of peak pressure $\Delta p/\rho_0 c_0$ [graph (a)] and the rise time $\Delta\tau$ [graph (b)] calculated at different receiver distances are plotted in Fig. 6. The rise time is calculated as the time portion between 10% and 90% of the peak pressure of the total waveform. According to this definition, we note that the rise time is essentially determined by the differences in arrival times of the eigenrays when more than one eigenray is present. The peak pressure always decreases in the presence of turbulence. For the Gaussian correlation function, there is a small difference between the temperature and the velocity turbulence. At a distance of $x/L=40$ a decrease of 25% is observed. For the random scalar field (temperature) this effect is more pronounced when the field is modeled using a von Kármán spectrum.[30] For this case the generated random field is more realistic since the inertial range extends over two decades. On average the rise time is always increased by turbulence. The curves start to deviate from the no turbulence case when the rays pass through the first caustic. Using Eq. (18) we evaluate the diffusion coefficient for the scalar field $\mathcal{D}_{2,c}$ and the vectorial field $\mathcal{D}_{2,v}$ and then estimate the distance x of the peak of the probability density function, i.e., $x=1.33\mathcal{D}_2^{-1/3}$. For the Gaussian turbulence fields we have $x_T^G=0.324$ m ($x_T^G/L\simeq 13$) for the temperature and $x_v^G=0.186$ m ($x_v^G/L\simeq 7.4$) for the velocity. The occurrence of the first caustic at shorter distances for the velocity field explains the quicker departure from the no turbulence values. In the case of the temperature fluctuations modeled with a von Kármán spectrum [Eq. (6)], the maximum of the probability density function appears at $x_T^K=0.522$ m, i.e., $x_T^K=5.22\,L_0$. We note that the increase of the rise time is significant as soon as the propagation distance x/L reaches the estimated distance of the maximum of the probability density function.

The histograms of peak pressure and rise time for Gaussian temperature fields are shown in Fig. 7 for four

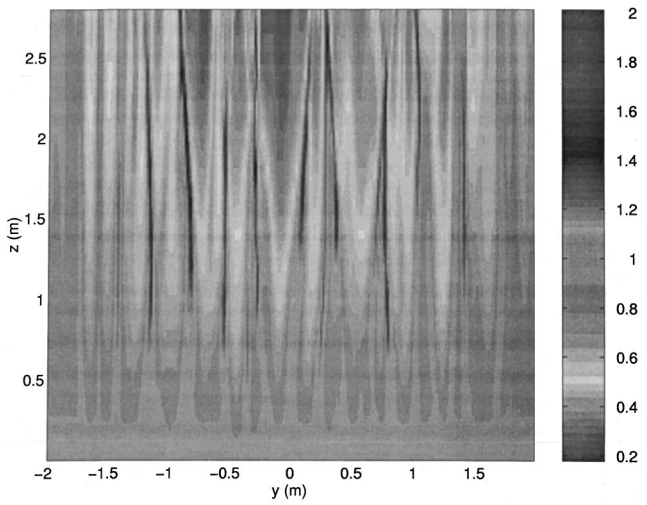

FIG. 9. Locations of peak pressure maxima of the wave obtained with the modified KZK approach.

propagation distances: $10\,L$, $20\,L$, $30\,L$, and $40\,L$. The solid line in each graph represents the no turbulence values of peak pressure and rise time. We observe that the distribution is asymmetric and that on average more peak pressures occur having values lower than for no turbulence. At the same time, a few large peak pressures are always present. Highest peak pressures are about twice that of the no turbulence value. The spread in peak pressure increases with propagation distance. The rise time distribution is also asymmetric and rise time is almost always increased by turbulence. With increasing propagation distance, large rise time values occur once the rays have passes through the first caustic. Maximum rise time values are an order of magnitude larger than the no turbulence value. Conclusions from the histograms are qualitatively the same as those from the model experiment with electrical sparks.[27]

B. Modified KZK approach

Our main interest in the use of a nonlinear parabolic wave equation was to study the evolution of the wave shape during its propagation in the turbulent media. A second motivation was to compare the effects of absorption and nonlinearity with the linear propagation effects. The initial plane wave parameters were equal to those used in the geometrical acoustics approach. The temperature fluctuations were modeled with 200 Fourier modes and a Gaussian turbulent spectrum ($L=0.1\,\mathrm{m}$ and $\theta'=4.27\,\mathrm{K}$). The length scale corresponded to that of an experiment used to study the influence of thermal turbulence on phase fluctuations and in particular on the role played by random caustics on the occurrence of shocks in the wave front of the transmitted pressure field.[31–33]

First, we compare the results from the geometrical and KZK approach with regard to the location and appearance of caustics. The caustics are purely geometrical acoustic results, i.e., infinite amplitudes predicted at foci in the absence of diffraction. In the KZK approach, the effect of diffraction limits the value of the peak pressure at the focus of the wave.[34] However, at the focus, a high peak pressure is still

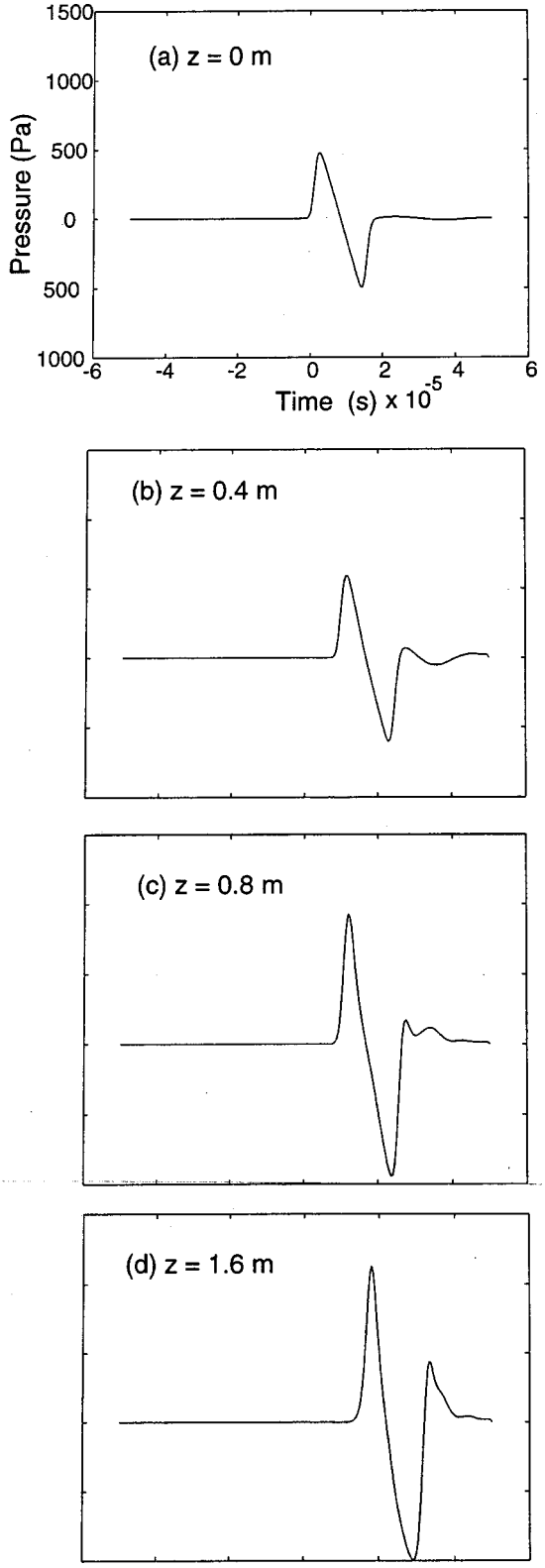

FIG. 10. Evolution of the N wave before and at a caustic. Calculation was done with the modified KZK approach for a Gaussian temperature field: (a) $z=0.0\,\mathrm{m}$, (b) $z=0.4\,\mathrm{m}$, (c) $z=0.8\,\mathrm{m}$, and (d) $z=1.6\,\mathrm{m}$.

obtained. In Figs. 8 and 9, we compare the value of the pressure maxima of the wave for the KZK approach case to the position of the caustics determined by the ray tracing approach. In Fig. 8, each dot represents the location of the first caustic along a ray path, and in Fig. 9 a map of the

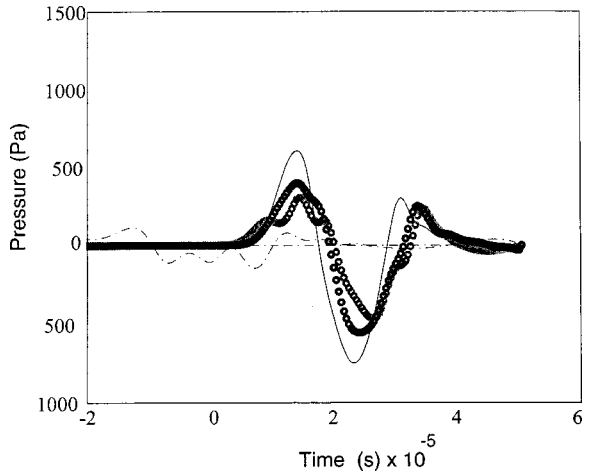

FIG. 11. Evolution of the *N* wave after propagation through a caustic. Calculation was done with the modified KZK approach for a Gaussian temperature field: (——) $z=2.0$ m, (●) $z=2.4$ m, (○) $z=2.8$ m, (–·–) $z=3.2$ m.

maximum pressure of the sound pulse is presented for each point in the spatial domain. Good agreement is seen between the position of the caustic and the maximum of the peak pressure. The agreement at the boundaries of the spatial domain is not as good because of the suppression of the turbulence field by the filter.

Next, we focus on the evolution of the *N* wave as it passes through one random caustic. The change of the waveform is shown in Fig. 10. The initial *N* wave is shown in graph (a). Graphs (b) and (c) show the waveform as it is propagating toward the caustic. We observe that the waveform becomes peaked. At the caustic [graph (d)] the biggest increase in peak pressure at the front and tail shock is observed. After the wave has passed through this caustic (Fig. 11), the wave is further distorted because it undergoes a phase shift. For large distances beyond the caustic ($z=3.2$ m) the wave front is no longer well defined because of the randomness of the propagating medium.

After propagating a certain distance through the turbulent medium, the wave shape can exhibit a wide variety of distortions. The effects that cause the distortion of the waveform are passage through a caustic, nonlinearity, and dissipation effects. In Fig. 12, examples of typical waveform distortion are shown. Figure 12 (a) shows the initial waveform. The rounded wave shape (graph b) occurs in an area where the sound speed is higher than c_0. In this case, the acoustical energy is transported from this area to a focusing area, and this process results in a decrease of the peak pressure. The nonlinear effects are weaker and the rise time increases compared with the no turbulence case. The peaked wave (graph c) occurs at a caustic as explained in the previous paragraph. A double peaked wave (graph d) is due to the superimposition of two consecutive wave fronts having slightly different

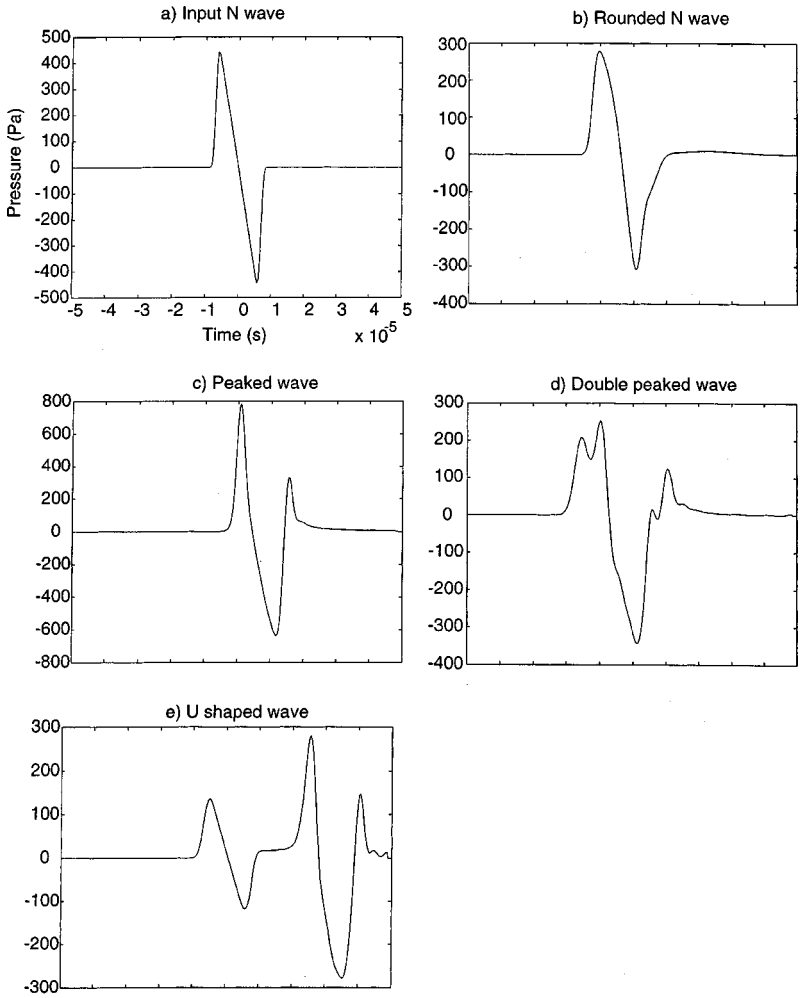

FIG. 12. Examples of distorted waveforms obtained with the modified KZK equation: (a) initial *N* wave, (b) rounded waveform, (c) peaked waveform, (d) double peaked waveform, and (e) U-shaped waveform.

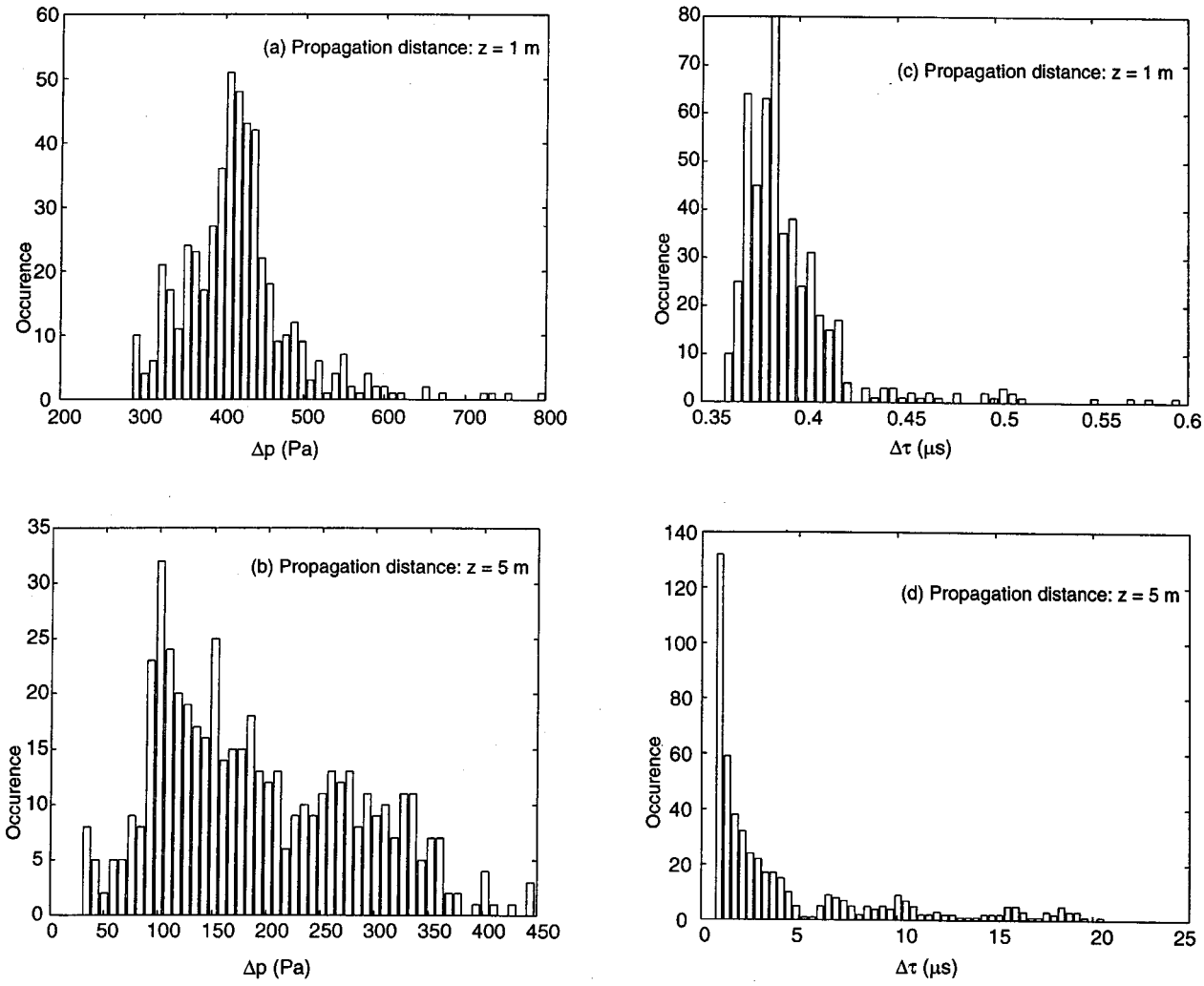

FIG. 13. Histograms of the peak pressure amplitude [(a) and (b)] and rise time [(c) and (d)] at a distance $z=1$ m and $z=5$ m from the source: results obtained with the modified KZK equation.

propagation times. A U-shaped waveform (graph e) is observed after a wave passes through a caustic.

Figure 13 shows the histograms of the peak pressure [graphs (a) and (b)] and rise time [graphs (c) and (d)] for two propagation distances $z=1$ m and $z=5$ m. For a propagation distance of $z=1$ m (i.e., $10L$) the expression for the probability of occurrence of the first caustic [Eq. (15)] indicates that only a few caustics exist. However, the distance of $z=5$ m (i.e., $50L$) is 3.85 times greater than the distance corresponding to the maximum of the probability density function ($x_T^G/L \simeq 13$). The distribution for the peak pressure is asymmetric and the mean peak pressure is smaller than the no turbulence case ($\overline{P}=430$ Pa at $z=1$ m; $\overline{P}=340$ Pa at $z=5$ m). The rise time histograms show that the turbulence almost always causes the rise time to increase when propagation distances increase. At the large distance $z=50L$, we note the appearance of a significant number of large values of the rise time. These conclusions are similar to those obtained with the geometrical acoustics method.

In order to obtain statistical information of peak pressure and rise time of the N waves, a spatial average over the y-direction of the computational domain was calculated for each realization. In Fig. 14, the average peak pressure amplitude [graph (a)] and rise time [graph (b)] are shown as a function of the propagation distance. Results are shown for three realizations of the turbulent field. It is observed that the average peak pressure decreases with increasing propagation distance. This decrease is also observed in the no-turbulence case and is caused by the effects of dissipation and relaxation. However, for the turbulence case, this decrease is more rapid and is in agreement with the results obtained in the geometrical approach (Fig. 6). This decrease is due to the focusing of the wave, since focusing also increases the dissipation rate. Moreover, the wave loses its coherence after propagation through a caustic, thereby increasing the duration and decreasing the peak pressure. The mean rise time increases with propagation distance. This result is in agreement with results of the geometrical acoustics approach. In absence of turbulence, rise time is decreased by effect of nonlinearity. An abrupt change of the slope of rise time increase is seen at a distance of the first caustics 1.3 m. The fact that turbulence always seems to increase the rise time is in agreement with the results of the spark produced N waves. The focusing of the waves at caustics seems to be of primary importance in explaining this behavior.

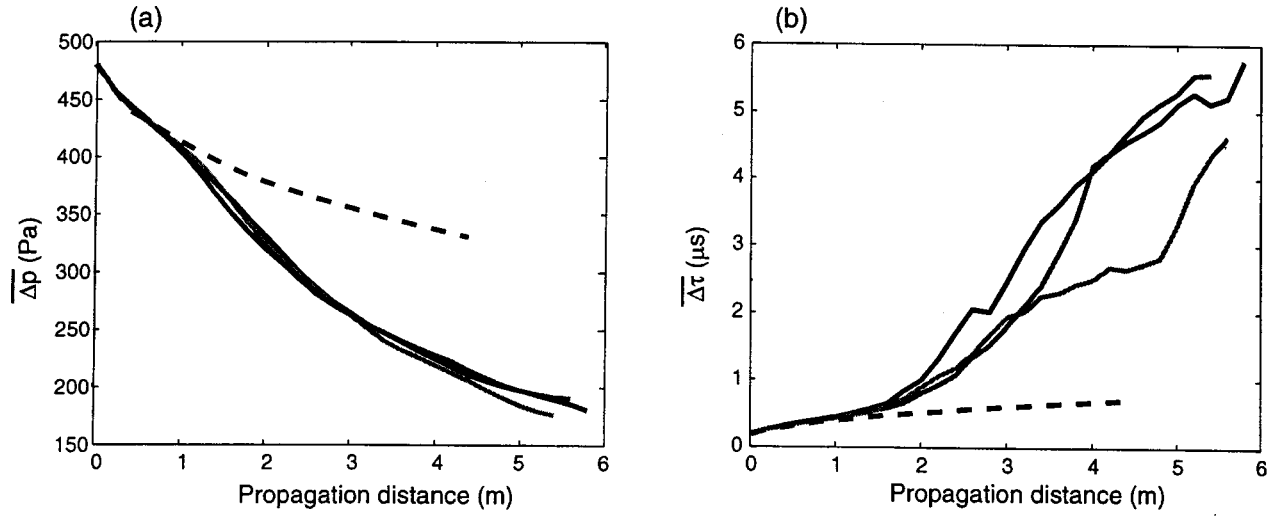

FIG. 14. Averaged peak pressure amplitude (a) and rise time (b) as a function of propagation distance: modified KZK equation. Results are shown for three realizations of a Gaussian turbulent field. The dashed line is the result for the no turbulence case.

VII. CONCLUSION

Two models are presented that describe nonlinear acoustic propagation through turbulence. The first model is based on a geometrical acoustics approach, in which a nonlinear transport equation is solved along the eigenrays. The second model is a modification of the nonlinear parabolic KZK equation. The modification is the inclusion of a random temperature field. Both models are then solved for individual realizations of a turbulent temperature or velocity field. The calculations are repeated and statistics are calculated.

The effect of turbulence on the waveform distortion, rise time, and peak pressure is calculated. It is shown that the nonlinear distortion in the presence of turbulence is weaker than without it. On average, peak pressure decreases in the presence of turbulence, and rise time increases. Peak pressure and rise time distributions are asymmetric. The effect of a velocity turbulence is more pronounced than that of a temperature field. The results confirm the observations of the model experiment.[27] We observed the same waveform distortion as was observed in the model experiment.[26]

In addition we calculated the probability density function for the occurrence of caustics. We showed that the location of caustics calculated by the geometrical acoustics method coincide with the peak pressure maxima calculated by the KZK method. The occurrence of caustics is shown to be responsible for the distortion of the waveform and the increase in variability of peak pressure and rise time.

ACKNOWLEDGMENTS

This research was supported in part by NATA Grant No. CRG941145. Funds for the first author were provided by a post-doctoral fellowship of the French Ministry of Education. C. Simand and P. Chary are gratefully acknowledged for their assistance with the numerical simulations. The authors gratefully acknowledge the many helpful suggestions provided by the reviewers.

[1] A. Niedzwiecki and H. S. Ribner, "Subjective loudness of *N*-wave sonic booms," J. Acoust. Soc. Am. **64**, 1622–1626 (1978).

[2] J. D. Leatherwood and B. M. Sullivan, "Subjective loudness response to simulated sonic booms," Proceedings, High-Speed Research Workshop on Sonic Boom, NASA Langley Research Center, Hampton, Virginia, edited by C. M. Darden, Vol. I, pp. 151–170 (1992).

[3] Y.-S. Lee and M. F. Hamilton, "Time-domain modeling of pulsed finite-amplitude sound beams," J. Acoust. Soc. Am. **97**, 906–917 (1994).

[4] Ph. Blanc-Benon, D. Juvé, and G. Comte-Bellot, "Occurrence of caustics for high-frequency acoustic waves propagating through turbulent fields," Theor. Comput. Fluid Dyn. **2**, 271–278 (1991).

[5] F. M. Pestorius, "Propagation of plane acoustic noise of finite amplitude," ARL Technical Report No. 73-23, Applied Research Laboratories, The University of Texas at Austin (AD 778868) (1973).

[6] G. Comte-Bellot, C. Bailly, and Ph. Blanc-Benon, "Modeling tools for flow noise and sound propagation through turbulence" in *New Tools in Turbulence Modeling*, edited by O. Métais and J. Ferziger (Les Editions de Physique Springer, 1997), pp. 141–162.

[7] J. O. Hinze, *Turbulence* (McGraw-Hill, New York, 1959).

[8] Y. H. Pao, "Transfer of turbulence energy and scalars quantities at large wave numbers," Phys. Fluids **11**, 1371–1372 (1968).

[9] A. D. Pierce, *Acoustics: An Introduction to Its Physical Principles and Applications* (McGraw-Hill, New York, 1981).

[10] S. M. Candel, "Numerical solution of conservation equations arising in linear wave theory: Application to aeroacoustics," J. Fluid Mech. **83**, 465–493 (1977).

[11] Ph. Blanc-Benon, D. Juvé, V. E. Ostashev, and R. Wandelt, "On the appearance of caustics for plane sound wave propagation in a moving random media," Waves Random Media **5**, 183–199 (1995).

[12] A. V. Kulkarny and B. S. White, "Focusing of waves in turbulent inhomogeneous media," Phys. Fluids **25**, 1770–1784 (1982).

[13] V. I. Klyatskin, "Caustics in random media," Waves Random Media **3**, 93–100 (1993).

[14] L. D. Robinson, "Sonic boom propagation through an inhomogeneous, windy atmosphere," Ph.D. dissertation, Physics Department, University of Texas at Austin (1990).

[15] D. Ludwig, "Uniform asymptotic expansions at a caustic," Commun. Pure Appl. Math. **19**, 215–250 (1966).

[16] D. T. Blackstock, "Generalized Burgers equation for plane waves," J. Acoust. Soc. Am. **77**, 2050–2053 (1985).

[17] P. Boulanger, R. Raspet, and H. E. Bass, "Sonic boom propagation through a realistic turbulent atmosphere," J. Acoust. Soc. Am. **98**, 3412–3417 (1995).

[18] V. W. Sparrow and A. D. Pierce, "Simulations of sonic boom ray tube area fluctuations for propagation through atmospheric turbulence including caustics via a Monte Carlo method," in *High Speed Research, Sonic Boom Volume I*, NASA Conference Publication 3172, edited by C. M. Darden (1992), pp. 49–62.

[19] R. O. Cleveland, J. P. Chambers, H. E. Bass, R. Raspet, D. T. Blackstock, and M. F. Hamilton, "Comparison of computer codes for the propagation

of sonic boom waveforms through isothermal atmospheres,'' J. Acoust. Soc. Am. **100**, 3017–3027 (1996).
[20] A. A. Piascek, ''A numerical study of weak step shocks that focus in two dimensions,'' Ph.D. dissertation, Department of Aerospace and Mechanical Engineering, Boston University, Massachusetts (1995).
[21] A. D. Pierce, ''Propagation of Acoustic Pulses and Sonic Booms through Small-Scale Atmospheric Turbulence,'' *16th AIAA Aeroacoustics Conference*, pp. 95–105, Munich (1995).
[22] O. V. Rudenko and V. A. Khokhlova, ''Statistics of sawtooth acoustic waves with random spatial modulation,'' Acoust. Phys. **40**, 111–115 (1994).
[23] R. O. Cleveland, M. F. Hamilton, and D. T. Blackstock, ''Time-domain modeling of finite-amplitude sound in relaxing fluids,'' J. Acoust. Soc. Am. **99**, 3312–3318 (1996).
[24] D. Juvé, Ph. Blanc-Benon, and P. Chevret, ''Sound propagation through a turbulent atmosphere: Influence of the turbulence model,'' in Proceedings of the Sixth International Symposium on Long Range Sound Propagation, Ottawa, Canada, pp. 270–282 (1994).
[25] B. Lipkens, ''Experimental and theoretical study of the propagation of *N* waves through a turbulent medium,'' Ph.D. dissertation, Department of Mechanical Engineering, University of Texas at Austin (1993).
[26] B. Lipkens and D. T. Blackstock, ''Model experiment to study sonic boom propagation through turbulence. Part I: Model experiment and general results,'' J. Acoust. Soc. Am. **103**, 148–158 (1998).
[27] B. Lipkens and D. T. Blackstock, ''Model experiment to study sonic boom propagation through turbulence. Part II: Effect of turbulence intensity and propagation distance through turbulence,'' J. Acoust. Soc. Am. **104**, 1301–1309 (1998).
[28] B. Lipkens and Ph. Blanc-Benon, ''Propagation of finite amplitude sound through turbulence: a geometrical approach,'' *Comptes Rendus Académie des Sciences Paris* T. 320, Série 2, pp. 477–484 (1995).
[29] B. Lipkens and Ph. Blanc-Benon, ''Numerical model for weakly nonlinear propagation of sound through turbulence,'' in High Speed Research, 1994 Sonic Boom Workshop, Atmospheric Propagation and Acceptability Studies, NASA Conference Publication 3279, edited by D. A. McCurdy (1994), pp. 61–80.
[30] C. Simand, ''Propagation d'un bang sonore dans l'atmosphere turbulente,'' Master Thesis, Ecole normale supérieure de Lyon (1996).
[31] Ph. Blanc-Benon and D. Juvé, ''Statistical properties of acoustic waves propagating through turbulent thermal fields,'' AIAA Paper No. 87-2727 (1987).
[32] Ph. Blanc-Benon and D. Juvé, ''Intensity fluctuations of spherical acoustic waves propagating through thermal turbulence,'' Waves Random Media **3**, 71–83 (1993).
[33] Ph. Blanc-Benon and D. Juvé, ''Dislocations in the wavefront of acoustic waves propagating through thermal turbulent fields,'' Forum Acusticum, Berlin, Acta Acustica CD-Rom 'Berlin99' ISBN3-9804568-5-4 (1999).
[34] A. T. Cates and D. G. Crighton, ''Nonlinear diffraction and caustic formation,'' Proc. R. Soc. London, Ser. A **430**, 69–88 (1990).